Available online at www.sciencedirect.com

SciVerse ScienceDirect

Journal of the European Ceramic Society 32 (2012) 2697–2703

www.elsevier.com/locate/jeurceramsoc

Introduction to a tough, strong and stable Ce-TZP/$MgAl_2O_4$ composite for biomedical applications

E. Apel [a], C. Ritzberger [a], N. Courtois [b,c], H. Reveron [b,c], J. Chevalier [b,c], M. Schweiger [a], F. Rothbrust [a], V.M. Rheinberger [a], W. Höland [a,*]

[a] *Ivoclar Vivadent AG, Bendererstr. 2, LI-9494 Schaan, Liechtenstein*
[b] *INSA-Lyon, MATEIS UMR5510, F-69621 Villeurbanne, France*
[c] *Université de Lyon, CNRS, France*

Available online 7 March 2012

Abstract

The processing of a new ceria-doped tetragonal zirconia polycrystal-based (Ce-TZP) composite and its microstructural and mechanical features are presented. Slip casting and die pressing were used to process commercially available Ce-TZP and $MgAl_2O_4$ powders into a dense ceramic composite. The absence of tetragonal to monoclinic transformation under hydrothermal conditions was assessed during accelerated aging tests. Biaxial flexural strength and fracture toughness values of more than 900 MPa and 15 MPa $\sqrt{m}$, respectively were measured, showing that phase transformation toughening of zirconia is maintained in the composite, while the inter/intragranular dispersion of nano-scaled magnesia spinel leads to strengthening of the Ce-TZP matrix. Flaw tolerance is attained, since the strength appears to be transformation dependent. These properties allow the composite to be used in the fabrication of various load-bearing components by employing conventional processing methods and sintering, for example for structural biomedical applications.

Keywords: Zirconia; Spinel; Composites; Strength; Toughness and toughening

1. Introduction

The most important developments in the field of high-tech ceramics have been mainly focused on the improvement of strength in the 1980s, then in both strengthening and toughening in the past two decades, considering that both properties were important in practice to produce load bearing and flaw tolerant products.

Among the technical oxide ceramics, zirconium oxide has played a major role since the 1980s. Its application as a sintered ceramic extends from medical uses to other technical applications. Zirconium oxide is capable of transforming from a tetragonal to a monoclinic phase, which toughens and strengthens the material.[1–4] This phenomenon is generally referred to as phase transformation toughening. A large number of materials and composites based on zirconia are available today. The largest group by far includes partially stabilized zirconium oxides and in particular tetragonal zirconia polycrystals (TZP) doped with the most popular stabilizing elements, i.e. yttrium and cerium. Depending on the type and percentage of the stabilization agent, the resulting mechanical properties differ quite considerably. Due to its high fracture toughness and its excellent durability to hydrothermal degradation (aging), ceria-doped zirconia has gained in popularity over the past few years.[5–9] It is however generally reported that Ce-TZP exhibits moderate strength as compared to Y-TZP, especially because of larger grains and a high propensity to stress induced phase transformation. As consequence, Y-TZP has been generally preferred for most applications. However, some possible issues concerning aging in service have been raised, which have had practical negative consequences in different applications.[8,9]

The strength of ceramics can be considerably increased by means of finely distributed secondary phases, such as those in ceramic nano-composites.[10–12] Moreover, grain boundary strengthening and the refinement of the microstructure have a positive effect on the mechanical characteristics of the ceramics.[13–15] Composites consisting of components such as alumina, zirconia, titanates, niobates and aluminates (including

* Corresponding author.
E-mail address: wolfram.hoeland@ivoclarvivadent.com (W. Höland).

0955-2219/$ – see front matter © 2012 Elsevier Ltd. All rights reserved.
doi:10.1016/j.jeurceramsoc.2012.02.002

spinel in particular), therefore represent a group of interest. These materials are characterized by their higher strength or toughness compared with the properties of the pure ceramic matrix.[16–23] A very tough and strong nano-composite, developed by Nawa et al.,[12] is based on Ce-stabilized zirconium oxide and 30 vol% alumina with a grain size of <200 nm. Its microstructure is composed of homogenously distributed nano-crystals of both the main components. It exhibits a fracture toughness of ~9.8 MPa $\sqrt{m}$ at a mean strength of 950 MPa. In 2005, another nano-crystalline composite composed of 3Y-TZP and 30 vol% $MgAl_2O_4$, possessing a flexural strength of 2200 MPa, was described by Morita et al.[11] It was processed by spark plasma sintering for the purpose of refining the microstructure.

In the present study, a new type of zirconia matrix composite based on a Ce-TZP–magnesium spinel system is proposed with the aim of providing both high toughness and strength and perfect stability under hydrothermal conditions. Samples with 16 vol% magnesium-spinel in a 10 Ce-TZP matrix were processed by slip-casting or die-pressing of spray-dried granules with simple technologies applicable to industrial, large scale production. Microstructure refinement of Ce-TZP together with improvement in strength has been studied. An overview of the critical defect size is given. Furthermore, the ability of the material to withstand intrinsic and extrinsic defects is discussed. Finally, the slow crack growth and aging behavior of the material is examined, with the aim of giving a full picture of the overall reliability of such new composites for biomedical or other high-tech applications.

2. Materials and methods

2.1. Green body preparation

To ensure a consistent quality of the test specimens, two commercial powders were used: 10 CeO_2-stabilized zirconia powder from Daiichi Kigenso Kagaku Kogyo Co., Ltd., Japan (CEZ-10-1; BET ~18–25 m^2/g) and $MgAl_2O_4$ from Baikowski, France (Baikalox® S30CR; BET ~30 m^2/g). The two powders were weighed according to a ratio of 90:10 (amounting to 16 vol% $MgAl_2O_4$ in the sintered composites) and dispersed with an electrosteric dispersant (Dolapix® CE64, Zschimmer & Schwarz, Germany). For both processing methods, 70 wt% solid content water-based slurries were prepared. Milling was conducted for several hours with zirconia beads. Slip casting was performed in porous Millecast® plaster moulds (Lafarge Prestia, France). Samples were dried at room temperature in ambient air.

Granulation was performed using a 35 kHz ultrasonic spraying nozzle (Synetude, France) in a co-current spray-drier, with 3 wt% polymer addition. The resulting powder was compacted into green bodies by uniaxial pressing with 200 MPa.

2.2. Sintering and sample preparation

Particular attention was paid to debinding, which was carried out with very low heating rates (<1 K/min) up to 600 °C. Subsequently, pre-sintering was performed at 1000 °C for 2 h, which yielded to specimens with Vickers hardness (HV0.5) between 550 and 800 MPa, allowing samples to be optimally shaped by further grinding or polishing for mechanical testing. Once the specimens were prepared according to the requirements for mechanical testing, they were pressureless sintered in air at 1400 °C/2 h using a heating and cooling rate of 10 K/min.

2.3. Measurement techniques

Phase analysis in the composite was carried out after sintering on as-fired surfaces by room-temperature X-ray diffraction (RT-XRD) using CuKα radiation. Diffractograms were obtained between 10 and 60° (2-theta angle) with a D5005 diffractometer (Bruker AXS, Karlsruhe, Germany). Microstructural examinations by scanning electron microscopy (SEM) were performed in a Supra 40VP microscope (Carl Zeiss NTS GmbH, Germany). For the slip cast specimens, as-cast surfaces were used. For die-pressed samples, a polished (1 μm) and thermally etched surface (1320 °C/10′) was investigated.

After each processing step (green body preparation and pre-sintering) the geometric bulk densities were measured. The final density was determined using the Archimedes method.

Low temperature degradation (LTD) was investigated on three samples of the composite after accelerated aging in steam at 134 °C, 2 bar according to ISO13356. In addition to the standard examinations, long-duration tests were performed, and one side of each sample was carefully ground and polished down to 1 μm diamond polishers after sintering. The monoclinic phase content of zirconia was determined by X-ray diffraction using Garvie's equation[24] on both polished and as-fired surfaces and compared with Y-TZP (Tosoh TZ-3Y-E grade) prepared under the same conditions.

Biaxial flexural strength was measured according to ISO 6872-2008. The sintered test specimens (13-mm diameter, 1.2-mm height) were finally prepared by pre-grinding with SiC-paper (1000 grit). Since at least 15 samples from each processing method were tested, a Weibull analysis was performed on the strength results. Vickers hardness was measured with 294 N load as HV30 (Vickers Indenter FV-700, Testwell, France).

Fracture toughness (K_{Ic}) and crack growth rate versus stress intensity (V–K_I) curves were obtained with the double-torsion method. A detailed description of the specimen geometry and loading conditions was published earlier in Chevalier et al.[25] The same testing method, with similar sample geometry and testing conditions was used in our previous works dedicated to oxide polycrystalline ceramics. As a result, a direct comparison with existing references was possible. The specimens consisted of plates measuring 40 mm × 20 mm × 2 mm. The tensile surface was polished with diamond pastes down to 1 μm grade, in order to view the crack with a precision of ±4 μm. A notch measuring $a_o = 10$ mm and root $\rho = 0.15$ mm was machined with a diamond saw. Subsequent pre-cracking was performed by loading the specimens at a low rate in order to induce a sharp crack of an initial length of $a_i = 13$ mm. The double torsion configuration is known for imparting stress intensity independent of crack length. However, we have shown in previous studies that the

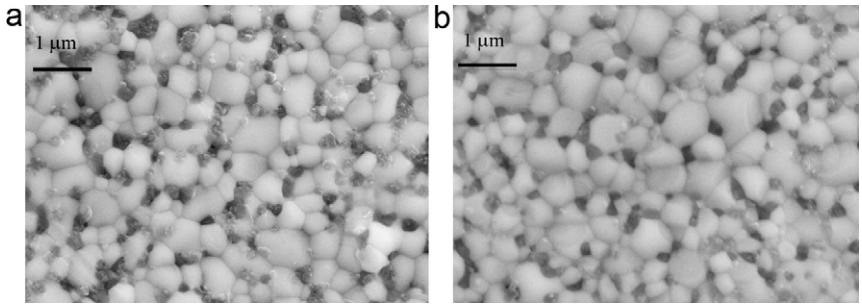

Fig. 1. Microstructure of 10 Ce-TZP–(16 vol%) $MgAl_2O_4$ composites obtained by slip casting (a) and die pressing (b).

stress intensity factor is slightly dependent on the crack length. Thus, the following more accurate expression was preferred:

$$K_I = H \cdot P \cdot \left(\frac{a}{a_o}\right)^{(6/32)} \quad (1)$$

In this equation, a is the total crack length, a_o is the notch length, P is the applied load and H is the standard geometrical factor for double torsion:

$$H = \frac{W_m}{U^2}\left(\frac{3(1+\nu)}{W \cdot \psi}\right) \quad (2)$$

where W_m is the moment arm, W is the width of the specimen, U is the thickness, ν is the Poisson ratio and ψ is a calibrating factor.[25]

For measuring the toughness, the specimens were loaded at a high rate (5 mm/min) in order to minimize slow crack growth before failure. In addition, the maximum stress intensity factor was recorded.

Slow crack growth was determined with two methods, namely constant loading tests and relaxation tests. The load relaxation method does not permit very low velocity measurements, but has the advantage of being faster. In principle, a full curve can be recorded in a single experiment. Pre-cracked specimens were rapidly loaded to a certain load value at which the displacement was kept constant. The relaxation curve (load versus time) and the crack length deduced from a compliance calibration curve were used to determine the V–K_I curve. One single relaxation test enables the determination of the entire V–K_I diagram in the velocity range of 10^{-7}–10^{-2} m/s.[25] The measurement of crack velocities under constant load presents the advantage of allowing very low velocities. In this case, the specimens were subjected to different static loads for the prescribed duration Δt. The crack length was measured by optical microscopy with a precision of ±4 µm and the crack velocity, V, defined as the ratio of the crack increment Δa to the test duration. Constant loading tests were therefore conducted to investigate crack growth rates lower than 10^{-5} m/s.

3. Results

3.1. Microstructure and phase analysis

After final sintering at 1400 °C/2 h, the XRD patterns of the bulk ceramic composite showed tetragonal 10 Ce-TZP (according to the XRD reference pattern ICDD 88-2395) as the main crystal phase. Cubic $MgAl_2O_4$ (according to ICDD 01-1154) was identified as a secondary phase. The monoclinic zirconia phase was negligible (below 1 vol%).

Fig. 1 shows the typical microstructures of the composite, obtained with the two processing methods. The well-dispersed spinel phase (dark) is clearly visible, consisting mainly of isolated grains within the zirconia matrix (light). This indicates that the second phase was de-agglomerated and well dispersed during slurry preparations. The microstructures obtained by the two methods are similar. Ce-TZP crystals measure 500 ± 250 nm, which is three times smaller than a ceramic consisting of pure Ce-TZP sintered at similar temperatures.[26] Spinel crystals measure from some dozens of nm to about 200 nm. Most of them are located at the grain boundaries. However, some images revealed that they may also be embedded in zirconia grains. Additionally very fine zirconia crystals were analyzed within the spinel grains, visible by using "inLens"-mode of scanning electron microscope (Fig. 2). Finally the composite posseses an inter-/intragranular microstrucure with submicron-nano-scaled crystals.

Even if the microstructures of the two types of samples were similar at small scale, pictures from fractured surfaces revealed that a few pressing defects of some micrometers were still present in the uniaxially pressed samples and were not sealed during sintering (see Fig. 3). The presence of these defects is common in pressed materials that are not subjected to further

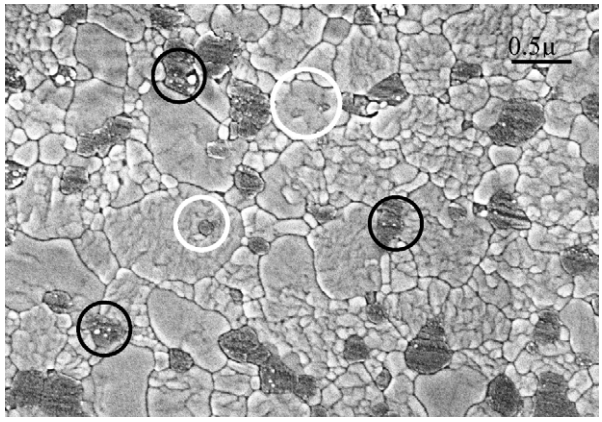

Fig. 2. Nano-scaled spinel crystals embedded within zirconia grains (white circles) and nano-scaled zirconia within spinel grains (black circles); thermal etched at 1300 °C 15 min (SEM-inLens observations).

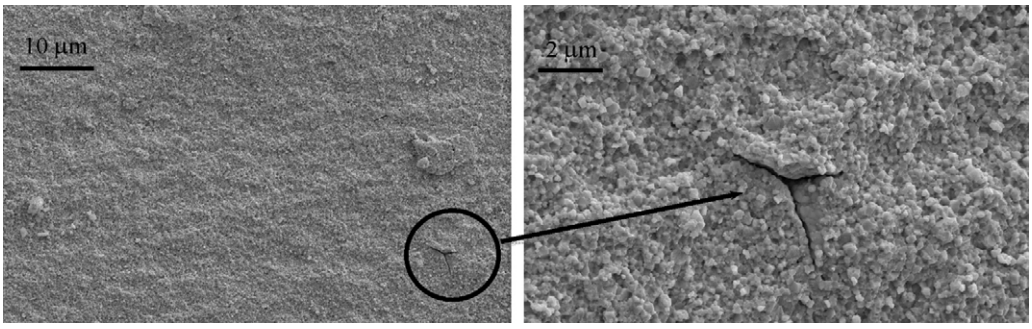

Fig. 3. Fracture surface of a sintered sample obtained via die pressing, revealing the presence of isolated pressing defects SEM.

Hot Isostatic Pressing (HIP). Such defects were not observed in the slip cast samples.

3.2. Relative densities depending on the processing step

The densities of slip cast and pressed samples at different stages of the process are listed in Table 1. Values are given as the relative density. For the composite 10 Ce-TZP containing 16 vol% magnesium-spinel, the theoretical density is 5.78 g/cm^3. It was calculated based on a rule of mixtures between tetragonal 10 Ce-TZP (6.195 g/cm^3, according to ICDD 88-2395) and spinel (3.579 g/cm^3, according to ICDD 01-1154) densities.

Higher green body densities were obtained by slip casting (56%), which is known to lead to a more homogeneous green microstructure. The green density of pressed samples reached 49%. It is noteworthy that even if the pressability of the granules (hence green density achieved) was acceptable, the organic composition of the granules was not specifically optimized for this study. Finally, all the samples attained a relative density of 98.7–99.9% after natural sintering without any help of HIP or pressure-assisted sintering technology.

3.3. Stability versus aging

Fig. 4 shows the evolution of the monoclinic fraction versus time during LTD tests. The aging kinetics of 10 Ce-TZP/$MgAl_2O_4$ composites were very slow in comparison with 3Y-TZP, irrespective of the surface preparation (as-sintered or polished). Forty-five hours of treatment at 134 °C was necessary to measure a slight increase in the monoclinic content of the as-sintered composite, which would represent approximately 180 years in the same environment at human body temperature, based on extrapolations proposed by Chevalier et al.[7,8] Hence, this material is nearly stable in the presence of water (or biological fluids) in the time-scale of medical or engineering applications near ambient temperatures. The present results show the beneficial effect of the (compressive) residual stresses induced by polishing, either in the composite or Y-TZP, in agreement with previous work.[27]

Table 1
Relative densities of slip-cast and pressed specimens at different stages of the process.

	Slip casting	Die pressing (200 MPa)
Green body	56.0%	49.2%
Pre-sintered body 1000 °C 2 h	58.4%	53.1%
Dense body 1400 °C 2 h	99.9%	98.7%

3.4. Mechanical properties

A mean hardness value of 10.4 ± 0.1 GPa was determined by Vickers indentation. Pronounced transformation relief was observed surrounding the indentation, which highlighted the high transformability of the material. The absence of cracking, even with such a high indentation loads (294 N), prevented any toughness determination based on an analysis of the crack system, but already showed a very high surface defect tolerance.

Regardless of the processing method used, a mean biaxial flexural strength of more than 900 MPa was reached by the new ceramic composite. Fig. 5 shows the probability of failure versus applied stress obtained for both processing techniques. Experimental data were expressed according to the Weibull distribution:

$$P_i = 1 - \exp\left(-\left(\frac{\sigma_i}{\sigma_m}\right)^m\right) \quad (3)$$

where P_i is the probability of failure under applied stress σ_i, and m and σ_m are the Weibull modulus and characteristic strengths.

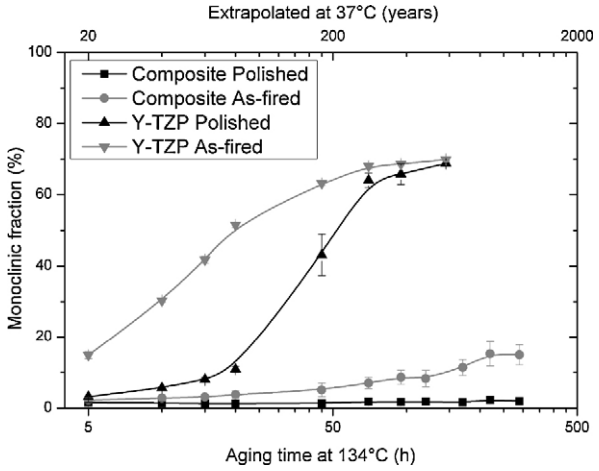

Fig. 4. Aging resistance of Y-TZP and 10 Ce-TZP/$MgAl_2O_4$ composite.

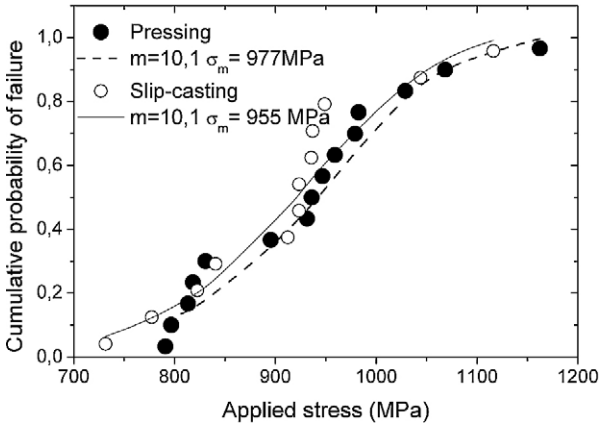

Fig. 5. Probability of failure versus applied stress for pressed and slip cast specimens. Continuous and dotted lines represent the fit of experimental data with Eq. (3).

Weibull moduli of $m = 10.1$ and characteristic strengths σ_m of 977 MPa and 955 MPa were obtained for pressed and slip cast samples respectively. Optical microscopy examinations with Nomarski Interference Contrast were conducted at different stages of loading for some samples. These investigations revealed transformation bands, which developed well before failure (around 80% of the maximum stress) and extended as the stress increased. A micrograph of such transformation bands taken at 90% of the stress-to-failure of a given sample is shown in Fig. 6. The composite therefore exhibits significant transformation before failure, as observed previously for pure 9 Ce-TZP or 10 Ce-TZP.[28] The difference is that the composite begins to transform at stresses that are higher than those previously reported for monolithic 10 mol% Ce-TZP (transformation at a stress lower than 340 MPa in biaxial bending).[28]

The K_{Ic} values were estimated by employing the double torsion method. Values above 15 MPa $\sqrt{m}$ were obtained independently of the processing method used. The plot of the crack growth rates versus the stress intensity factor obtained by load relaxation and constant stress tests gives an overview of the

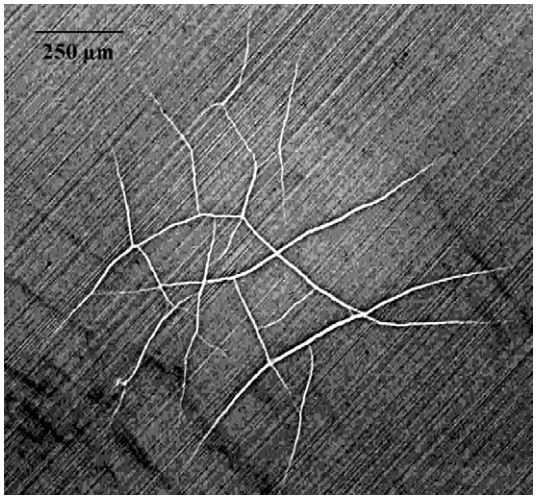

Fig. 6. Transformation zones observed on the tensile surface of a specimen prior to failure (90% of stress to failure).

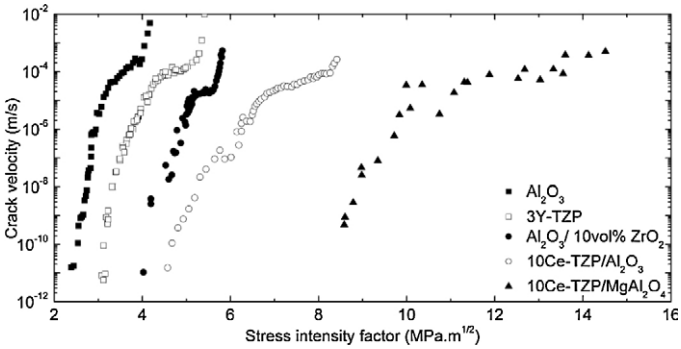

Fig. 7. V–K_I curve of the 10 Ce-TZP–magnesium aluminate spinel composite, compared to alumina, 3Y-TZP, alumina–10 vol% zirconia[31] and Ce-TZP–alumina nano-composite.[29]

composite crack resistance (Fig. 7). Three different stages are identified, corresponding to environmentally stress induced corrosion mechanisms, as reported for other oxide ceramics.[7] The threshold stress intensity factor, below which no significant crack propagation occurs, is estimated to be close to 8 MPa $\sqrt{m}$. In comparison to existing materials, the entire range of crack velocity shifted to higher K_I values.

An overview of materials properties is given in Table 2. For comparison, values of other typical oxide ceramics have been taken from reference publications.[29–31]

4. Discussion

The combination of a tough zirconia matrix with an evenly dispersed secondary phase has produced a special combination of strength and toughness in this 10 Ce-TZP/$MgAl_2O_4$ composite. Pure ceria-doped zirconia, which is prone to phase transformation toughening, can exhibit high fracture toughness (especially for a ceria content lower than 12 mol%), but limited strength. The strength values generally reported so far for pure Ce-TZP have been on the order of 600–700 MPa.[32] As highlighted by Swain and Rose[33] highly transformable zirconia ceramics, such as monolithic 10 Ce-TZP, show moderate strength, limited by the stress at which transformation first proceeds. In other words, 10 Ce-TZP exhibits a t-m transformation before crack propagation, and the maximum sustainable stress is ruled by the stress for transformation. This is interesting in terms of reliability and flaw tolerance, but a significant drawback in terms of maximum sustainable loading of structural pieces. High fracture toughness (higher than 15 MPa $\sqrt{m}$) and biaxial flexural strength (above 900 MPa) were measured on the composite samples processed by two different methods: slip casting and die pressing. The fact that transformation occurred at the sample surface well-before failure demonstrates that the strength of the composites is still transformation driven. Higher strength than that generally reported for pure 10 mol% ceria-doped zirconia shows that the transformability is therefore decreased by the addition of spinel particles. Further work would be necessary to define the main origin of a lower transformability, since a smaller grain size and the presence of a stiffer second phase both lead to a lower tendency to transform. In spite of this lower

Table 2
Compared properties of different oxide ceramics.

Material	Toughness (K_{Ic}, MPa $\sqrt{m}$) double-torsion	Biaxial flexural strength (MPa)	Weibull modulus	Critical defect size a_c (μm)
Alumina	4.2[31]	687[34]	7[34]	12
3Y-TZP	6[25]	1280[30]	5.7[30]	7
10 Ce-TZP	15–20[26]	500[26 a]		>200
12 Ce-TZP	8[29]	540[26 a]		40
10 Ce-TZP/Al_2O_3	8.8–11.8[29]	1330[30]	6.7[30]	14–25
10 Ce-TZP/$MgAl_2O_4$ (slip-casting)	>15	910 ± 105	10.1	>110
10Ce-TZP/$MgAl_2O_4$ (die pressing)	>15	930 ± 110	10.1	

[a] Measured by four-point bending.

transformability, toughness is still preserved and comparable to that of pure 10 Ce-TZP. The preferred presence of nano-scaled spinel grains in a quantity close to the percolation threshold is thought to be in part responsible for the mechanical behavior of this material. Furthermore, single nano-scaled spinel crystals were found to be embedded within the zirconia grains. They may also have contributed to the toughening and strengthening of the material.

To provide an idea of the critical flaw size (a_c) in this ceramic composite, a simple calculation was made based on the Griffith equation (4).

$$K_{Ic} = \sigma_f . \sqrt{(\pi . a_c)} \quad (4)$$

Extraordinary values of ~120 μm critical defect size were attained. These values are one order of magnitude above those found for Y-TZP, and the flaws are also much larger than the processing defects visible in the die pressed samples (Fig. 2).

The fact that the calculated critical flaw size is significantly larger than the flaws observed experimentally in both types of samples (cast or pressed) entirely agrees with the finding that transformation occurred before failure and that maximum sustainable stress is ruled by transformation (and not flaw propagation). Strength is therefore independent of the initial flaw distribution, provided the largest flaws are smaller than 120 μm. Despite a different flaw population between cast and pressed samples, the flexural strength (and calculated Weibull modulus) is the same. This is a very important advantage of such flaw tolerant materials. From a practical point of view, using this type of flaw tolerant submicron-nano-composite leads to an increase in the reliability of products and reduces the influence of pressing, machining and finishing steps on strength.

Another important aspect of such composites is their overall crack resistance behavior, which demonstrates higher K_I values as compared to alumina, zirconia and current generations of alumina–zirconia composites, and even to Ce-TZP – and the alumina nano-composites developed recently. More in-depth investigation on the presence and characterization of the threshold stress intensity factor is needed, but it is estimated to be around 8 MPa $\sqrt{m}$. This would mean that no delayed failure would be expected, even for stress intensity factors leading to immediate (or almost), rapid failure in all other ceramics.

Finally, the use of cerium as a dopant leads to almost fully stable zirconia based ceramics. In ceria-doped tetragonal zirconia polycrystals (Ce-TZP), Zr^{4+} substitution by Ce^{4+} does not create oxygen vacancies in the crystal lattice, as is the case in Y-TZP. Therefore, the degradation kinetics of Ce-TZP is very slow and negligible in the time scale of the application.[6] The presence of Spinel as a second phase does contribute to change mechanical properties of the material, but does not change its susceptibility to aging since the two phases are immiscible, and zirconia still only stabilized by Ce^{4+}.

The 10 Ce-TZP/$MgAl_2O_4$ composites introduced in this investigation are therefore an excellent alternative to current oxide ceramics and composites for structural applications such as dental restorations. The material easily satisfies all ISO 13356 requirements. Further developments may lead to an even better balance between strength and toughness, which could be achieved by slightly reducing the transformability of Ce-TZP grains to increase the maximum sustainable stress. This balance could also be adapted, depending on the application.

5. Conclusions

Two conventional processing methods, that is, slip casting and spray drying followed by die pressing, were successfully conducted for the manufacture of a new Ce-TZP/$MgAl_2O_4$ submicron-nano-composite. Biaxial flexural strength tests revealed no difference between the two processing methods, due to the high toughness of the material (>15 MPa $\sqrt{m}$). The designed composition with 84 vol% Ce-TZP maintained a high level of transformability of the composite. The combination of strength (900 MPa) and toughness was explained by the grain size reduction subsequent to inter- and intragranular dispersion of the nano-scaled spinel, which increased the critical stress of zirconia during the tetragonal to monoclinic transformation. Consequently, the new type of composite is a flaw-tolerant zirconia matrix composite, which is suitable for the production of structural ceramic products. Due to its resistance against low temperature degradation, the composite may be suitable for biomedical uses.

References

1. Lange FF. Transformation toughening. *J Mater Sci* 1982;**17**:247–54.
2. Basu B. Toughnening of yttria-stabilised tetragonal zirconia ceramics. *Int Mater Rev* 2005;**50**(4):239–56.
3. Deville S, Guénin G, Chevalier J. Martensitic transformation in zirconia. Part I. Nanometer scale prediction and measurement of transformation induced relief. *Acta Mater* 2004;**52**:5697–707.

4. Deville S, Guénin G, Chevalier J. Martensitic transformation in zirconia. Part II. Martensite growth. *Acta Mater* 2004;**52**:5709–21.
5. Chevalier J, Gremillard L, Virkar AV, Clarke DR. The tetragonal-monoclinic transformation in zirconia: lessons learned and future trends. *J Am Ceram Soc* 2009;**92**(9):1901–20.
6. Sato T, Shimada M. Control of the tetragonal-to-monoclinic phase transformation of yttria stabilized zirconia in hot water. *J Mater Sci* 1985;**20**:3988–92.
7. Chevalier J, Gremillard L. Ceramics for medical applications: a picture for the next 20 years. *J Eur Ceram Soc* 2009;**29**:1245–55.
8. Chevalier J, Gremillard L, Deville S. Low-temperature degradation of zirconia and implications for biomedical implant. *Annu Rev Mater Res* 2007;**37**:1–32.
9. Lance MJ, Vogel EM, Reith LA, Cannon WR. Low-temperature aging of zirconia ferrules for optical connectors. *J Am Ceram Soc* 2001;**84**(11):2731–3.
10. Niihara K. New design concept of structural ceramics–ceramic nanocomposites. *J Ceram Soc Jpn* 1991;**99**(10):974–82.
11. Morita K, Hiraga K, Kim BN, Yoshida H, Sakka Y. Synthesis of dense nanoscrystalline ZrO_2–$MgAl_2O_4$ spinel composite. *Scr Mater* 2005;**53**:1007–12.
12. Nawa M, Nakamoto S, Sekino T, Niihara K. Tough and strong Ce-TZP/alumina nanocomposites doped with titania. *Ceram Int* 1998;**24**:497–506.
13. Wang J, Ponton CB, Marquis PM. The grain boundary modification of ceria-stabilized tetragonal zirconia polycrystals by a small amount of alumina addition. *J Mater Sci Lett* 1993;**12**:702–5.
14. He YJ, Winnubst AJA, Sagel-Ransijn CD, Burggraff AJ, Verweij H. Enhanced mechanical properties by grain boundary strengthening in ultrafine-grained TZP ceramics. *J Eur Ceram Soc* 1996;**16**:601–12.
15. Mukhopadhyay A, Basu B. Consolidation–microstructure–property relationships in bulk nanoceramics and ceramic nanocomposites: a review. *Int Mater Rev* 2007;**52**(5):257–88.
16. Nevarez-Rascon A, Aguilar-Elguezabal A, Orrantia E, Bocanegra-Bernal MH. One the wide range of mechanical properties of ZTA and ATZ based dental ceramic composites by varying the Al_2O_3 and ZrO_2 content. *Int J Refrac Mat Hard Mater* 2009;**27**(6):962–70.
17. Quenard O, Laurent CH, Peigney A, Rousset A. Zirconia-spinel composites. Part II: mechanical properties. *Mater Res Bull* 2000;**35**:1979–87.
18. Ganesh I, Ferreira JMF. Synthesis and characterization of $MgAl_2O_4$–ZrO_2 composites. *Ceram Int* 2009;**35**:259–64.
19. Cutler RA, Mayhew RJ, Prettyman KM, Virkar AV. High-toughness Ce-TZP/Al_2O_3 ceramics with improved hardness and strength. *J Am Ceram Soc* 1991;**74**:179–86.
20. Miura M, Hongoh H, Yogo T, Hirano S, Fuji T. Formation of plate-like lanthanum-β-aluminate crystal in Ce-TZP-matrix. *J Mater Sci* 1994;**29**:262–8.
21. Yang B, Chen XM, Liu XQ. Effect of $BaTiO_3$ addition on structures and mechanical properties of 3Y-TZP ceramics. *J Eur Ceram Soc* 2000;**20**:1153–8.
22. Chen XM, Liu XQ, Liu F, Zhang XB. 3Y-TZP ceramics toughened by $Sr_2Nb_2O_7$ secondary phase. *J Eur Ceram Soc* 2001;**21**: 477–81.
23. Yuh SD, Lai YC, Chou CC, Lee HY. $YNbO_4$-addition on the fracture toughness of ZrO_2(3Y) ceramics. *J Mater Sci* 2001;**36**:2303–11.
24. Garvie RC, Nicholson PS. Phase analysis in zirconia systems. *J Am Ceram Soc* 1972;**55**(6):303–5.
25. Chevalier J, Saadaoui M, Olagnon C, Fantozzi G. Double-torsion testing a 3Y-TZP ceramic. *Ceram Int* 1996:171–7.
26. El Attaoui H, Saadaoui M, Chevalier J, Fantozzi G. Static and cyclic crack propagation in Ce-TZP ceramics with different amounts of transformation toughening. *J Eur Ceram Soc* 2007;**27**(2–3):483–6.
27. Deville S, Chevalier J, Gremillard L. Influence of surface finish and residual stresses on the ageing sensitivity of biomedical grade zirconia. *Biomaterials* 2006;**27**(10):2186–92.
28. Rauchs G, Fett T, Munz D, Oberacker R. Tetragonal-to-monoclinic phase transformation in CeO_2-stabilized zirconia under multiaxial loading. *J Eur Ceram Soc* 2000;**22**(6):841–9.
29. Benzaid R, Chevalier J, Saadaoui M, Fantozzi G, Nawa M, Diaz LA, et al. Fracture toughness, strength and slow crack growth in a ceria stabilized zirconia–alumina nanocomposite for medical applications. *Biomaterials* 2008;**29**:3636–41.
30. Fischer J, Stawarczyk B. Compatibility of machined Ce-TZP/Al_2O_3 nanocomposite and a veneering ceramic. *Dent Mater* 2007;**23**: 1500–5.
31. De Aza AH, Chevalier J, Fantozzi G, Schehl M, Torrecillas R. Crack growth resistance of alumina, zirconia and zirconia toughened alumina ceramics for joint prostheses. *Biomaterials* 2002;**23**: 937–45.
32. Tsukuma K, Shimada M. Strength, fracture toughness and Vickers hardness of Ce-TZP. *J Mater Sci* 1985;**20**:1178–84.
33. Swain MV, Rose LRF. Strength limitations of transformation-toughened zirconia alloys. *J Am Ceram Soc* 1986;**69**(7):511–8.
34. Wagner WC, Chu TM. Biaxial flexural strength and indentation fracture toughness of three new dental core ceramics. *J Prosthet Dent* 1996;**76**(2):140–4.